Effect of Heat Input Parameters on Molten Pool Size during Selective Laser Melting of Ti-6Al-4V Powder Through Numerical Simulation

Liang Zhang[1], Kaiqi Wu[1], Qiyun Yang[1], Xiaoqing Ni[1], Tao Wang[1], Wenheng Wu[1,*] and Lin Lu[1,*]

[1] Shanghai Engineering Research Center of 3D Printing Materials, Shanghai Research Institute of Materials, Shanghai 200437, China
[*]E-mail: wwhwwh2004@126.com; Lulinws@163.com

Abstract. Numerical simulations were proposed to research the influence of heat input parameters on the melting pool dimension and temperature field distribution during the selective laser melting process of Ti-6Al-4V powder. Firstly, temperature field results demonstrate that in the same powder layer, the center part of the sample will experience three more obvious heating processes under the irradiation of laser. Secondly, a good exponential function relationship is found between the melting pool dimension and volume energy density. Finally, based on the melting pool dimension from our numerical simulations, two full-process energy prediction diagrams are drawn to predict hatch spacing and powder layer thickness of SLM Ti-6Al-4V powder, consistent with the experimental results.

1. Introduction

Selective laser melting (SLM) technique can directely fabricate complex parts from three-dimensional CAD data without any extra tools.[1,2] Compared with transitional subtractive manufacturing, SLM has a high level of flexibility, meaning that it can deal with various commercial metal powder materials, for example, Ti-6Al-4V.[3-5]

In SLM process, temperature filed, determined by heat input parameters such as laser power and scanning velocity, has great influence on micro-structures and mechanical properties of parts considerably. Therefore, it is crucial to study the temperature field during SLM process of Ti-6Al-4V powder. However, SLM process involves numerous complex physicochemical phenomena, which could not be revealed clearly by traditional experimental method.[6]

Finite element methods are adopted to address this problem.[7-10] In this study, a three-dimensional finite element model is firstly constructed to investigate the influence of heat input parameters on melting pool dimension and temperature field in the process of SLM Ti-6Al-4V powder. Secondly, two full-process energy prediction diagrams of SLM Ti-6Al-4V powder are plotted by the values of simulated melting pool dimension.

2. Finite Element Modeling Method

The model of SLM Ti-6Al-4V powder based on finite element method is constructed and shown in figure 1. The below block with a dimension of 1.96×1.12×0.20 mm^3 is considered as the stain-steel substrate and the upper block with a dimension of 1.12×0.56×0.09 mm^3 is regarded as the powder bed of Ti-6Al-4V, in which the powder bed is evenly divided into three layers of 0.03 mm each.

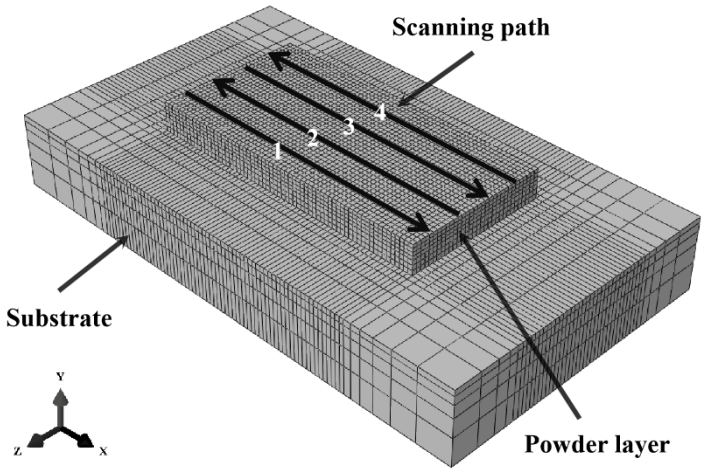

Figure 1. Three-dimensional finite element model of SLM Ti-6Al-4V powder

To save simulation resource and maintain enough precision, the Ti-6Al-4V powder bed is meshed by fine grids with dimensions of 0.0175×0.0175×0.01 mm^3 while the stainless-steel substrate is meshed by coarser grids. The coarser mesh dimension gradually increases with the distance from the Ti-6Al-4V powder bed increasing.

Considering the laser penetration depth and instantaneous heat transfer during SLM process of Ti-6Al-4V powder, a Gaussian distribution heat source is chosen and mathematically presented as, [11]

$$q(x,y,z)=\frac{\eta\cdot 6\sqrt{3}Q}{hr^2\pi\sqrt{\pi}}exp\left(-\frac{3x^2}{r^2}-\frac{3y^2}{r^2}-\frac{3z^2}{h^2}\right) \quad (1)$$

in which, the q (x, y, z) is the heat flux density of point (x, y, z), Q is the laser absorption of powder, η is the laser power, r is radius of surface of Gaussian heat source and h is depth of Gaussian heat source.

In addition, to better simulate the thermal interaction between the powder and solidified layer, the thermophysical properties of the powder layer and solidified alloy material are temperature-dependent. The chemical compositions and thermal physical properties of Ti-6Al-4V are summarized in table 1 and table 2, respectively.

Table 1. Chemical compositions of Ti-6Al-4V

Element	Ti	Al	Fe	V	C	O
Compositions (wt.%)	89.53	6.09	0.11	4.03	0.01	0.12

Table 2. Thermal physical properties of Ti-6Al-4V at various temperatures

Temperature °C	Density g·cm^{-3}	Specific heat J/(g·K)	Conductivity W/(m·K)
25	4.425	0.548	5.845
300	4.390	0.625	11.180
600	4.346	0.720	15.934
900	4.312	1.177	21.496
1200	4.280	0.694	27.418
1500	4.220	0.766	32.230
1800	3.991	0.977	101.082

Finally, a FORTRAN program is written not only to control the magnitude and moving path of Gaussian distribution heat source, but also to realize transition of material from powder to solid. Besides that, the hatch spacing is set to 0.12 mm, the different laser powers (*P*) are 250, 280 and 310 W, and the different scanning speeds (*v*) are 1100, 1200, and 1300 mm/s.

3. Results and Discussions

3.1 Effects of Heat Input Parameters on Temperature and Cooling Rate

The rapid cooling in the tiny melting pool, one of the important characteristics of SLM process, has a great influence on the formation of micro-structure and grain refinement of the alloy. This work systemically investigates the temperature and cooling rate of the forming process under different heat input. Figure 2a and 2b show the temperature curve with time under different laser powers (*P*) and scanning velocities (*v*), respectively. It can be found that the central area of SLM part will undergo three obvious heating processes, namely, the initial heating process of powder, the melting process of powder and the reheating process of solidification state. Secondly, when the laser scanning velocity is fixed at 1200 mm/s, the peak temperature increases gradually from 2812 to 3235 °C with the laser power increasing from 250 to 310 W, shown in figure 2a. Thirdly, when the laser power is fixed at 280 W, the peak temperature decreases gradually from 3086 to 2964 °C with the laser scanning velocity increasing from 1100 to 1300 mm/s, shown in figure 2b. To sum up, laser power and scanning velocity are two important parameters during SLM process, determining the temperature field distribution in forming process.

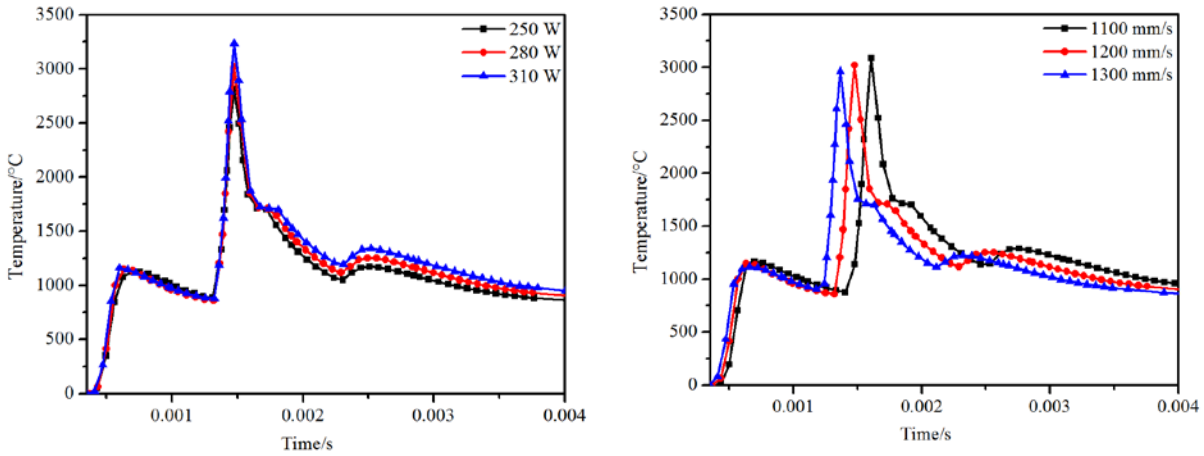

Figure 2. Temperature curve with time under different laser powers for *v*=1200 mm/s (a) and temperature curve with time under different scanning velocities for *P*=280 W (b)

3.2 Effects of Heat Input Parameters on Melting pool dimensions

As is well known, melting pool dimensions extremely affect the metallurgical bonding between the adjacent trajectories (and layers) during SLM process. For instance, if melting pool dimension is too large, it will cause balling effect; however, if melting pool dimension is too small, it will result in incomplete fusion. Therefore, the prediction of melting pool dimension is essential because it can guide the selection of the heat input parameters of SLM technology.

To better analyze the influence of various SLM processing parameters on melting pool dimension, it can be characterized by volume energy density, *E*, which is mathematically expressed as follows, [12]

$$E = \frac{P}{v \cdot s \cdot d} \tag{2}$$

in which P is laser power, v is laser scanning speed, s is laser scanning hatch spacing, and d is powder layer thickness. This section, a series of extra laser powers (100, 150, 200, 300, and 350 W) and scanning velocities (600, 900, 1500, and 1800 mm/s) are added to systematically research the influence of volume energy density on melting pool dimension.

Our simulated melting pool dimensions of SLM Ti-6Al-4V powder are showed in figure 3. It can be seen that a satisfactory exponential function relationship is found between the melting pool dimension and volume energy density, which is expressed as follows,

$$y = y_0 + A_1(1-e^{-x/t_1}) + A_2(1-e^{-x/t_2}) \tag{3}$$

where the parameters y_0, A_1, t_1, A_2, and t_2 are obtained at -79.15, 268.01, 28.23, 3.56, and 8.15 for melting pool width with R^2 values of 0.9692, and at -16.75, 42.32, 36.27, 1.13, and 3.17 for melting pool depth with R^2 values of 0.9811, respectively. In short, melting pool dimension increases with volume energy density increasing.

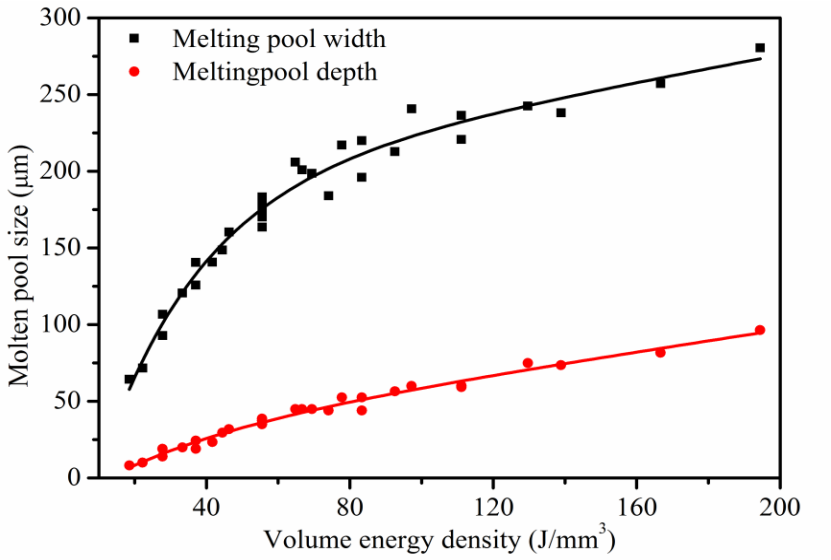

Figure 3. Effect of volume energy density on melting pool dimension

3.3 Full-Process Energy Prediction Diagrams of SLM Ti-6Al-4V Powder

It is well known that an appropriate overlap between neighbouring trajectories (and layers) is helpful to avert defect of SLM part, such as pore and crack. Presumably, the overlap between neighbouring trajectories is controlled by a combination of hatch spacing and melting pool width; the overlap between vertical trajectories in different layers is controlled by a combination of powder layer thickness and melting pool depth. Thus, based on the melting pool dimension calculated from our numerical simulations, two full-process energy prediction diagrams of SLM Ti-6Al-4V powder are drawn and demonstrated in figure 4.

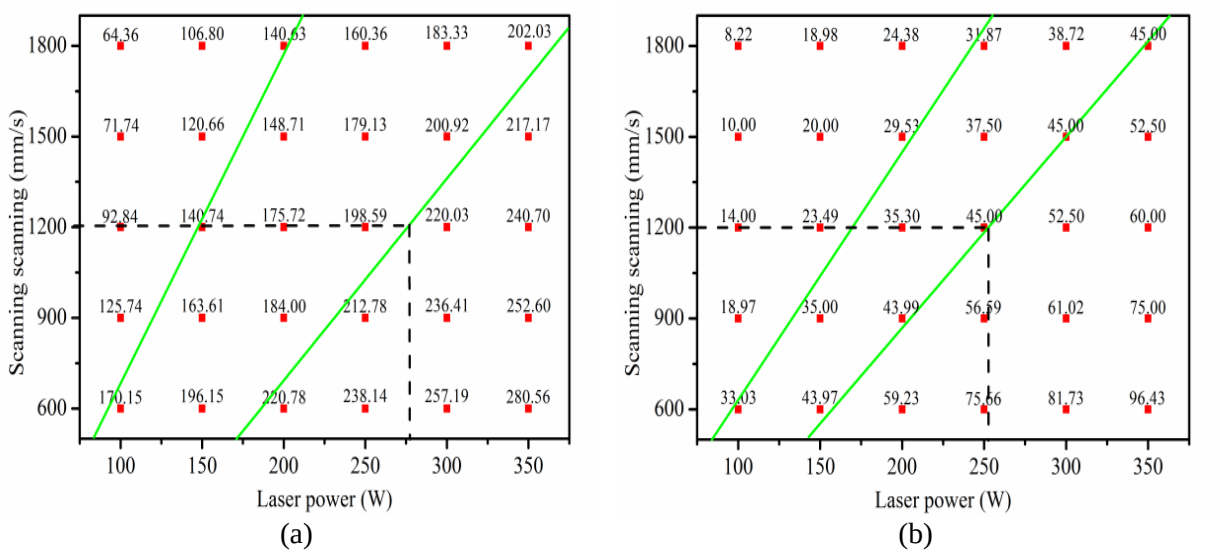

Figure 4. Two full-process energy prediction diagrams of SLM Ti-6Al-4V powder based on the our simulated (a) width and (b) depth of melting pool

In figure 4, these red points are melting pool dimensions calculated from our numerical simulations under the different laser powers and scanning velocities, the two green lines in figure 4a represent the melting pool width in the same level with values of 0.14 mm and 0.21 mm, and the two green lines in figure 4b represent the melting pool depth in the same level with values of 0.03 mm and 0.045 mm.

The hatch spacing and layer thickness of SLM Ti-6Al-4V powder can be predicted via these two diagrams. For example, if the laser power, scanning velocity, and powder layer thickness are set to 1200 mm/s, 280 W, and 0.03 mm, respectively, the corresponding melting pool width will be about 0.21 mm. In this situation, to obtain a fine metallurgical bonding between neighbouring trajectories in the same layer, the best hatch spacing should be set about 0.14 mm, almost consistent with real experiment, to overlap half of melting pool. Analogously, if the laser power, scanning velocity, and hatch spacing are 255 W, 1200 mm/s, and 0.12 mm, the corresponding melting pool depth will be about 0.045 mm. In this situation, to obtain a fine metallurgical bonding between neighbouring layers, the optimal layer thickness of Ti-6Al-4V powder should be set to about 0.03 mm, almost consistent with real experiment, to overlap half of melting pool.

Not only that, the diagram can be applied to select laser power and scanning speed in the same way, as well. To sum up, the plotted full-process energy prediction diagram provides a important guidance for selecting heat input parameters of SLM process.

4. Conclusions

In this work, numerial simulations are proposed to research the process of SLM Ti-6Al-4V powder. There are three important results. Firstly, laser power and scanning velocity are two important parameters, determining the temperature field of Ti-6Al-4V alloy in the SLM process. Secondly, there is a satisfactory exponential function between volume energy density and melting pool dimension and the melting pool dimension increases with the volume energy density. Thirdly, the plotted full-process energy prediction diagram provides a important guidance for selecting heat input parameters of SLM process.

5. Acknowledgments

This work is supported by the project to strengthen industrial development at the grass-roots level (Project Number TC160A310/19), and Shanghai Rising-star program (Project Number 18QB1400600).

6. References

[1] Ali H, Ghadbeigi H and Mumtaz 2018 *Mater*. *Sci*. *Eng*. A **712** 175
[2] Song J, Li X J, Zhang Y, Yan L M, Jiang T and Peng S M 2017 *J. Electrochem. Soc*. **164** 846
[3] Gu D D, Hagedron Y C, Meiners W, Meng G B and Poprawe R 2012 *Acta Mater.* **60** 3849
[4] Zhang Y, Song J, Yan L M, Shi S P and Peng S M 2019 *Electrchim, Acta* **239** 446
[5] Song J, Gao Z B and Zhang L 2019 *Mol. Simulat.* **45** 935
[6] Sun S B, Zheng L J Liu Y Y Liu J H and Zhang H 2015 *Int. J. Adv. Manuf. Technol.* **80** 1787
[7] Parry L A, Ashcroft I A and Wildman R D 2019 *Addit. Manuf.* **25** 166
[8] Song J, Zhang L, Wu W H, He B B and Lu L 2019 *J. Mater. Res.* **34** 1395
[9] Luo C, Qiu L, Yan Y, Yang J, Uher C and Tang X 2018 *J. Mater. Process. Tech.* **261** 74
[10] Li Y and Gu D D 2014 *Mater. Design* **63** 856
[11] Song B, Dong S J, Liao H L and Coddet C 2012 *Int. J. Adv. Manuf. Technol.* **61** 967
[12] Thijs L, Verhaeghe F, Craeghs T, Humbeeck J V and Kruth J-P 2010 *Acta Mater.* **58** 3303